Title

Enhanced exchange bias in IrMn/CoFe deposited on self-organized hexagonally patterned nanodots

Journal

Applied Physics Letters, 106(7)

ISSN

0003-6951

Authors

Li, WJ
Shi, DW
Greene, Peter K
et al.

Publication Date

2015-02-16

DOI

10.1063/1.4913422

Peer reviewed

Enhanced exchange bias in IrMn/CoFe deposited on self-organized hexagonally patterned nanodots

W. J. Li,[1] D. W. Shi,[1] Peter K. Greene,[2] K. Javed,[1] Kai Liu,[2,a)] and X. F. Han[1,b)]
[1]*Beijing National Laboratory for Condensed Matter Physics, Institute of Physics, Chinese Academy of Sciences, Beijing 100190, China*
[2]*Physics Department, University of California, Davis, California 95616, USA*

(Received 4 December 2014; accepted 11 February 2015; published online 20 February 2015)

Exchange biased nanostructures of IrMn/CoFe were deposited on anodized alumina with hexagonally patterned nanodot surface structures. Nanodots with diameters of 20, 70, and 100 nm were fabricated to investigate the size effect on the magnetic properties. Magnetometry and the first-order reversal curve method revealed significant enhancements of the exchange bias and coercivity in the nanodots compared with flat films. The enhancements can be attributed to the effective reduction of ferromagnet domain sizes and increased random fields due to the nanostructure morphology and domain wall pinning by the boundaries between adjacent nanodots. © *2015 AIP Publishing LLC*.
[http://dx.doi.org/10.1063/1.4913422]

The ferromagnetic/antiferromagnetic (FM/AF) exchange bias effect was first discovered by Meiklejohn and Bean in partially oxidized particles.[1] More recently, extensive efforts have been devoted to the fabrication and investigation of exchange biased nanostructures from both fundamental and technological points of view.[2–13] The continued size reduction of spintronic devices and the explosive growth of magnetic recording areal density have triggered intense interest in exchange biased nanostructures.[14] From the basic point of view, nanomaterials usually exhibit unique properties due to the reduction of the lateral dimensions.

While lithographic techniques have been widely used for the fabrication of isolated exchange biased nanostructures,[15,16] simple and inexpensive non-lithographic methods are highly attractive. Among them, pseudo-ordered structures of FM/AF bilayers deposited on pre-patterned substrates have been developed recently.[17,18] Although anodized aluminum oxide (AAO) templates are generally used for the fabrication of various one-dimensional nanomaterials, they have also been utilized to create nanodots[19] or networks[6,20] by depositing materials either into the pores or onto the surface of the AAO templates, respectively. Using AAO templates are a promising and convenient approach to achieve exchange biased nanostructures. However, there are still conflicting reports on the magnitude of the exchange bias effect in patterned structures, as compared to that in continuous films. Specifically, exchange bias has been found to increase in contiguous networks,[6,9,12] but decrease in isolated nanodots.[15] Thus, it is essential to carry out systematic studies on the exchange bias effect arising from the reduced sizes of the nanostructures. More recently, it has been shown that the self-organized hexagonally patterned nanodot arrays at the bottom of the AAO template can be used as new two-dimensional curved substrates to achieve nanostructures over macroscopic areas.[21]

In this letter, we report on the synthesis and study of FM/AF bilayers grown on self-organized hexagonally patterned nanodots, where we observe an enhanced exchange bias. The semi-spherical nanodots were formed during electrochemical anodization of ultra-pure aluminum foils (~99.999% purity, purchased from General Research Institute for Nonferrous Metals). Prior to anodizing, the foils were first electropolished in a 4:1 volume mixture of C_2H_5OH and $HClO_4$ to reduce the surface roughness. Though different acids (oxalic, sulfuric, and phosphoric acids) were used to fabricate AAO template with different pore diameters,[22,23] oxalic acid was the most common choice and used here. The anodization voltage was the primary control factor to tailor the nanodot size in this work. Similar to the fabrication of AAO template, a standard two-step anodizing procedure in 0.3 M oxalic acid solution at 0 °C was performed to obtain the aluminum oxide. The residual aluminum after the second anodization step was removed, and a hexagonally patterned nanodot surface was obtained. Polycrystalline FM/AF bilayers with the structure of Ta (2 nm)/IrMn (12 nm)/CoFe (5 nm)/Ta (2 nm) were deposited on the hexagonally patterned nanodot arrays with different diameters of 20, 70, and 100 nm by magnetron sputtering in a high vacuum chamber with a base vacuum of 10^{-6} Pa. The targets in our sputtering system were off axis and tilted, and the substrate was rotating and exposed in an in-plane magnetic field during deposition. The in-plane magnetic field was parallel to the substrate and rotating with it synchronously. The angle between the direction of deposition and the substrate is about 30°. Continuous thin films with the same structure were deposited on a thermally oxidized Si wafer for comparison. The morphologies of the hexagonally patterned nanodot arrays were characterized by scanning electron microscope (SEM) and atomic force microscopy (AFM). Magnetic properties of the FM/AF exchange biased nanostructures were measured by a vibrating sample magnetometer (VSM) at room temperature.

The structure and morphology of the FM/AF bilayer nanodot arrays are similar to those described in a prior publication.[21] Here, we just illustrate the nanodot arrays with the

a)Electronic mail: kailiu@ucdavis.edu
b)Electronic mail: xfhan@iphy.ac.cn

smallest diameter of 20 nm, characterized by AFM and shown in Fig. 1(a). The FM/AF bilayer clearly still maintains the hexagonally patterned dot nanostructure even though the total layer thickness is comparable to the height of the 20 nm nanodots. When the deposited flux arrives at the substrate at the 30° angle, it will form a strong shadowing effect in the valleys (boundaries between adjacent nanodots) because of the patterned nanodot arrays. Thus, the magnetic material is deposited mainly on top of the nanodots with little deposition around the valleys. Fig. 1(b) illustrates the formation of nanocaps on the surface of the curved substrate, which is confirmed by the cross-sectional profile determined from the AFM scan, as shown in Fig. 1(c). The morphology is similar to nanocap arrays fabricated by depositing on polystyrene (PS) colloid sphere templates reported earlier.[24]

Fig. 2 shows the easy axis normalized hysteresis loops of a continuous IrMn/CoFe film and the IrMn/CoFe bilayers deposited on the hexagonally patterned nanodot arrays with different diameters of 20, 70, and 100 nm. The unidirectional anisotropy was set by the magnetic field applied during deposition, as indicated in Fig. 1(a). The continuous bilayer film shows a coercivity of 180 Oe and an exchange bias of 344 Oe. Compared with the hysteresis loop of the continuous film, those of the exchange biased nanostructures are much more sheared. This is caused by the increased disorders in the nanocaps, which disrupt reversal as the size of the nanodots become smaller and the variable FM/AF thickness. Additionally, the caps also have a distribution of magnetic easy axis which contributes to the sheared loop shape.

The variations in exchange bias and coercivity of different samples are shown in Table I. The VSM results show that

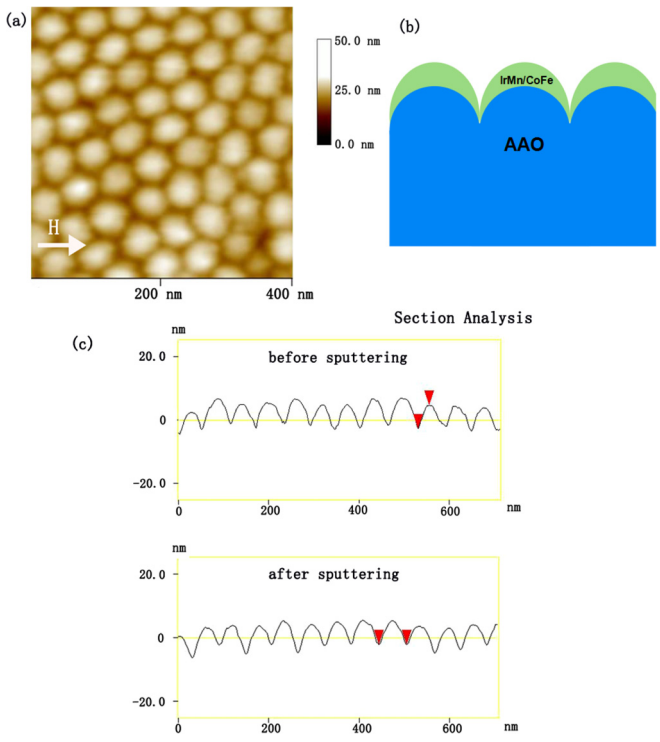

FIG. 1. The structure and morphology of the nanodot arrays. (a) A typical AFM image of the 20 nm nanodot arrays, after deposition of Ta (2 nm)/IrMn (12 nm)/CoFe (5 nm)/Ta (2 nm). (b) Schematic of the formation of nanocaps on the surface of the curved substrate. (c) Cross-sectional AFM analysis of the 20 nm nanodots before and after sputtering.

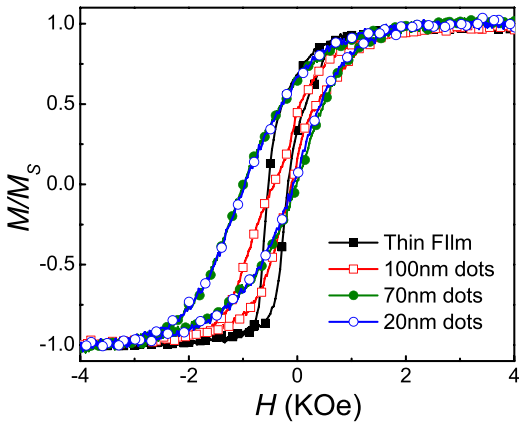

FIG. 2. In-plane magnetic hysteresis loops of continuous film and nanodots with different diameters of 20, 70, and 100 nm.

nanodots with diameters of 20 and 70 nm give enhanced H_E and H_C values compared to the continuous film, similar to earlier studies of exchange biased networks.[6,9,12] However, the 100 nm nanodots show a slight decrease both in H_E and H_C values. Previous theoretical studies on the coercivity mechanisms in FM/AF bilayers have demonstrated that the FM reversal is mainly dependent on the FM-FM exchange interaction between neighboring grains and the random field due to the FM/AF interfacial interactions.[5,25] The former is stronger than the latter in continuous thin films grown on a flat Si substrate, which results in large FM domains (often on the micron scale during reversal[5]) compared to AF grains, and the random field averages out to be small, leading to small H_E and H_C. In the case of FM/AF bilayers deposited on the nanodots, the thickness of the magnetic material deposited around the valleys is much smaller compared to the total thickness of the continuous thin films, and the layer structure is compromised. Thus, exchange coupling among the neighboring nanocaps is much weaker and each nanocap is expected to reverse its magnetization essentially independently, especially for the smaller nanodot sizes. As a result, the FM domains are forced to break down into much smaller sizes, leading to larger random fields and consequently larger H_E and H_C. Additionally, the domain-wall pinning caused by the non-uniform structure at the valleys of the nanodots contributes to a further enhancement of the coercivity. The seemingly abnormal drop in H_E and H_C for the 100 nm sized sample may be caused by the disordered valleys between the neighboring nanocaps and the insufficient pinning of the FM layer exerted by the reduced thickness of the AF layer in the valleys.[26]

To further investigate the magnetization reversal process, we have employed the first-order reversal curve

TABLE I. Exchange bias H_E and coercivity H_C measured by VSM in the easy axis direction, and bias field H_B and local coercivity H_C measured by FORC.

	Thin film	100 nm	70 nm	20 nm
VSM H_C(Oe)	180	160	491	450
VSM H_E(Oe)	−344	−260	−510	−526
FORC H_C(Oe)	220	420	800	650
FORC H_B(Oe)	−410	−700	−570	−620

(FORC) method, as described earlier.[27–31] The FORCs were measured with the field applied in the plane of the film/nanodots at room temperature. For each FORC, the sample was first saturated in a positive field; then the field was reduced to a particular reversal field H_r, and the magnetization was measured as the applied magnetic field H_a was increased back towards saturation. The sequence was repeated with decreasing values of the reversal field until negative saturation was reached. The FORC distribution was then extracted according to[32]

$$\rho(H_a, H_r) = -\frac{1}{2}\frac{\partial^2 M(H_a, H_r)}{\partial H_a \partial H_r}. \quad (1)$$

The FORC distribution eliminates purely reversible components of the magnetization switching and maps the reversal events in terms of local coercive field $H_C = (H_a - H_r)/2$ and interaction field $H_B = (H_a + H_r)/2$. Thus, the FORC distribution deconvolutes the properties of the measured ensemble, e.g., can be used to investigate magnetic phase evolutions.[33]

FORC distributions for both the continuous film and the exchange biased nanostructures with different nanodot sizes are shown in Fig. 3. For the thin film sample, the FORC distribution is centered at ($H_C = 220$ Oe and $H_B = -410$ Oe), consistent with the major loop coercivity of 180 Oe and exchange bias of −344 Oe. For nanodot samples, the FORC distribution is bimodal, consisting of two separate features. First, the main peak of the FORC distribution spreads more widely in both H_C and H_B (Figs. 3(b)–3(d)) with decreasing nanodot size. Spread in H_C indicates a larger variation of local domain pinning across the sample.[34] As the nanodots decrease in size, the ratio of dot "surface" vs. "valley" decreases. The valleys are both thinner and more disordered, inhibiting domain wall motion between dots and causing each dot to reverse locally. The variations in the magnetic easy axis within the nanocaps also contribute to the local coercivity spread. Likewise, the extension in H_B is attributed to the varied local interactions within the film causing different regions to be biased by different amounts. Interestingly, the main FORC peak is centered at much larger (H_C, H_B) values than those suggested by major loop measurements. For example, the bias field H_B in all three dot samples is consistently and substantially larger than that in the film sample (by 40%–70%, as shown in Table I). Second, the non-uniform thickness caused by the curved surface of the substrate is also manifested in the FORC distribution. In the valleys, the FM/AF interfaces are no longer well defined, and the layers are very thin. Thus, the AF component is unable to provide sufficient pinning of the FM layer, leading to a FORC feature with very little exchange bias and small coercivity, independent of the FM/AF structure deposited on the dot surface. This is quite clear in the bimodal FORC distributions for the nanodot samples (see Figs. 3(b)–3(d)), which is absent in the thin film sample (see Fig. 3(a)).

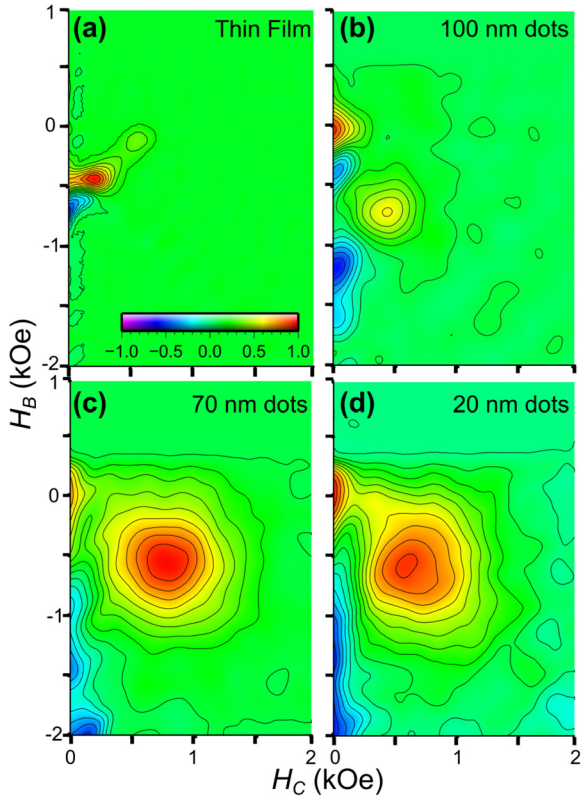

FIG. 3. FORC distributions of IrMn/CoFe bilayers deposited on different substrates: (a) continuous film, (b) 100 nm dots, (c) 70 nm dots, and (d) 20 nm dots. The FORC distribution is calculated using a continuous slope extension at the boundary, yielding only irreversible magnetization switching events. The distributions are normalized by their respective peak values.

It is interesting to compare the ensemble-averaged VSM results with the FORC distributions, which deconvolutes the contributions from the dot surfaces and valleys. For example, in the 100 nm dots sample, the VSM results show that both coercivity and exchange bias are slightly reduced compared with those in the continuous film. The main FORC distribution in this sample actually moves to higher H_C and H_B values compared with the continuous film, consistent with the enhancement seen in the 20 nm and 70 nm nanodot samples. However, there is a second FORC feature near ($H_C = 100$ Oe and $H_B = 0$ Oe), which corresponds to the disordered valley. This contribution is significant enough to cause an overall reduction in coercivity and exchange bias measured by VSM. In the 20 nm and 70 nm samples, contributions from the nanodot surfaces are dominant over those from the valleys, leading to larger coercivity and exchange bias measured by VSM. In the 20 nm dots, the coercivity value is slightly smaller than that in the 70 nm dots, as effects of thermal fluctuation start to be significant.

In summary, we have fabricated exchange biased nanostructure of IrMn/CoFe by using AAO templates with hexagonally patterned nanodot surface as pre-patterned substrates. Compared with the isolated exchange biased nanostructures fabricated by lithographic techniques, this self-assembly method is simple and cost-effective. Moreover, geometrical parameters of the self-organized hexagonally patterned nanodot arrays at the bottom of the AAO template can be easily controlled. These two-dimensional curved substrates serve as an interesting platform to study magnetic nanostructures. FM/AF bilayers were deposited on the self-organized hexagonally patterned nanodots with different diameters. Significant enhancements of H_E and H_C values were observed compared with the continuous flat film, revealed by FORC distributions of the nanodots and valleys. The formation of separate nanocaps on the surface of the nanodots impedes domain wall

propagation, giving rise to larger random fields and enhanced H_E and H_C. The curvature of the nanodot arrays induces strong modifications in the exchange biased nanostructures, which is quite interesting from both fundamental and technological points of view.

The project has been supported by the State Key Project of Fundamental Research and 863 Plan Project of Ministry of Science and Technology [MOST, Nos. 2010CB934401 and 2014AA032904], the National Natural Science Foundation of China [NSFC, Grant Nos. 11374351 and 11434014]. Work at UCD has been supported by the U.S. NSF (DMR-1008791 and ECCS-1232275).

[1]W. H. Meiklejohn and C. P. Bean, Phys. Rev. **102**, 1413 (1956).
[2]J. Nogués and I. K. Schuller, J. Magn. Magn. Mater. **192**, 203 (1999).
[3]A. E. Berkowitz and K. Takano, J. Magn. Magn. Mater. **200**, 552 (1999).
[4]S. M. Zhou, K. Liu, and C. L. Chien, Phys. Rev. B **58**, R14717 (1998).
[5]Z. Li and S. F. Zhang, Phys. Rev. B **61**, R14897 (2000).
[6]L. Sun, Y. Ding, C. L. Chien, and P. C. Searson, Phys. Rev. B **64**, 184430 (2001).
[7]J. Sort, A. Hoffmann, S.-H. Chung, K. S. Buchanan, M. Grimsditch, M. D. Baró, B. Dieny, and J. Nogués, Phys. Rev. Lett. **95**, 067201 (2005).
[8]J. Nogues, J. Sort, V. Langlais, V. Skumryev, S. Surinach, J. S. Munoz, and M. D. Baro, Phys. Rep. **422**, 65 (2005).
[9]K. Liu, S. M. Baker, M. Tuominen, T. P. Russell, and I. K. Schuller, Phys. Rev. B **63**, 060403 (2001).
[10]S. Laureti, S. Y. Suck, H. Haas, E. Prestat, O. Bourgeois, and D. Givord, Phys. Rev. Lett. **108**, 077205 (2012).
[11]V. Baltz, J. Sort, S. Landis, B. Rodmacq, and B. Dieny, Phys. Rev. Lett. **94**, 117201 (2005).
[12]M. T. Rahman, N. N. Shams, D. S. Wang, and C.-H. Lai, Appl. Phys. Lett. **94**, 082503 (2009).
[13]W. J. Gong, W. J. Yu, W. Liu, S. Guo, S. Ma, J. N. Feng, B. Li, and Z. D. Zhang, Appl. Phys. Lett. **101**, 012407 (2012).
[14]X. F. Han, S. S. Ali, and S. H. Liang, Sci. China: Phys., Mech. Astron. **56**, 29 (2012).
[15]V. Baltz, J. Sort, B. Rodmacq, B. Dieny, and S. Landis, Appl. Phys. Lett. **84**, 4923 (2004).
[16]M. Fraune, U. Rüdiger, G. Güntherodt, S. Cardoso, and P. Freitas, Appl. Phys. Lett. **77**, 3815 (2000).
[17]J. H. Yang, S. Y. Yang, M. B. Wei, Y. X. Wang, Y. J. Zhang, N. N. Yang, J. Li, S. S. Liu, W. Li, and X. T. Wu, Appl. Phys. A **108**, 363 (2012).
[18]Z. Shi, X. X. Fan, P. He, S. M. Zhou, H. N. Hu, M. Yang, and J. Du, J. Appl. Phys. **113**, 17D722 (2013).
[19]K. Liu, J. Nogués, C. Leighton, H. Masuda, K. Nishio, I. V. Roshchin, and I. K. Schuller, Appl. Phys. Lett. **81**, 4434 (2002).
[20]K. Liu and C. L. Chien, IEEE Trans. Magn. **34**, 1021 (1998).
[21]D. W. Shi, P. K. Greene, P. Liu, K. Javed, K. Liu, and X. F. Han, IEEE Trans. Magn. **50**, 2303004 (2014).
[22]O. Jessensky, F. Müller, and U. Gösele, Appl. Phys. Lett. **72**, 1173 (1998).
[23]J. P. Zhang, J. E. Kielbasa, and D. L. Carroll, Mater. Chem. Phys. **122**, 295 (2010).
[24]M. Albrecht, G. H. Hu, I. L. Guhr, T. C. Ulbrich, J. Boneberg, P. Leiderer, and G. Schatz, Nat. Mater. **4**, 203 (2005).
[25]Z. J. Li and S. F. Zhang, Appl. Phys. Lett. **77**, 423 (2000).
[26]V. Baltz, J. Sort, B. Rodmacq, B. Dieny, and S. Landis, Phys. Rev. B **72**, 104419 (2005).
[27]J. E. Davies, O. Hellwig, E. E. Fullerton, G. Denbeaux, J. B. Kortright, and K. Liu, Phys. Rev. B **70**, 224434 (2004).
[28]C. R. Pike, A. P. Roberts, and K. L. Verosub, J. Appl. Phys. **85**, 6660 (1999).
[29]R. K. Dumas, K. Liu, C. P. Li, I. V. Roshchin, and I. K. Schuller, Appl. Phys. Lett. **91**, 202501 (2007).
[30]X. M. Kou, X. Fan, R. K. Dumas, Q. Lu, Y. P. Zhang, H. Zhu, X. K. Zhang, K. Liu, and J. Q. Xiao, Adv. Mater. **23**, 1393 (2011).
[31]D. A. Gilbert, G. T. Zimanyi, R. K. Dumas, M. Winklhofer, A. Gomez, N. Eibagi, J. L. Vicent, and K. Liu, Sci. Rep. **4**, 4204 (2014).
[32]I. D. Mayergoyz, *Mathematical Models of Hysteresis* (Springer-Verlag, New York, 1991).
[33]D. A. Gilbert, J. W. Liao, L. W. Wang, J. W. Lau, T. J. Klemmer, J. U. Thiele, C. H. Lai, and K. Liu, APL Mater. **2**, 086106 (2014).
[34]J. W. Liao, R. K. Dumas, H. C. Hou, Y. C. Huang, W. C. Tsai, L. W. Wang, D. S. Wang, M. S. Lin, Y. C. Wu, R. Z. Chen, C. H. Chiu, J. W. Lau, K. Liu, and C. H. Lai, Phys. Rev. B **82**, 014423 (2010).